J. Phys. Res. Edu., Vol. 1, March 2024

# Spectral variability in the orbital profiles of TeV Binary $LSI + 61^o$ 303 in X-Ray window using $XMM - Newton$ Observations

Tamal Sarkar*

*HECRRC, University of North Bengal, Siliguri, WB 734 013 India*

$LSI + 61^o$ 303 is a high-mass X-ray binary consisting of a low-mass $[M\ (1-4)M_\odot]$ compact object orbiting around an early type B0 Ve star along an eccentric $e = 0.7$ orbit. It along with LS5039 are the only two known gamma-ray binary detected in the TeV band. Despite extensive observations the nature of this source, particularly whether it is a pulsar or a black hole (micro-quasar) system, is not clear. The mechanisms that lead to the multi-wavelength behavior are also uncertain. Recent approach to the study of $LSI + 61^o$ 303 has been to focus on possible correlated variability. There was an early indication that there is a correlation between the X-ray and TeV emission at the time where the latter was measurable. In a more recent observation, however, such a feature has not been found. In this work, we study the spectral variability of $LSI + 61^o$ 303 using four observations between 2001 to 2007 of $XMM - Newton$ available from NASA archive and examine the correlation between low energy range and high energy part.

## I. INTRODUCTION

The Be star binary $LSI + 61^o$ 303 is among the few X-ray binaries from which radio and very high-energy gamma-ray emission [1] in TeV energies were observed [2, 3]. Be stars are a heterogeneous collection of stars with B spectral types and emission lines. The radio source GT 0236 +601, is considered to be associated with this Be Star [4], the radio outbursts show a periodicity of about 26.496 days [4] and a further modulation of the outburst phase and outburst peak flux with a period of 1667 +/- 8 days [5]. This indicate that the position of the maximum of radio emission along the orbit with $P_{orb}$ = 26.496 days [4], as well as its intensity, are modulated with a super-orbital period [6] of $P_{sup}$ = 1667 days. Albert *et al* [7] found that the peak flux at TeV energies occurs at orbital phase $\phi_{orb} = 0.65$, while no high energy emission is detected around peri-astron passage $\phi_{orb} = 0.23$. Using VLBA imaging obtained by Dhawan *et al* (2006) over full orbit of LS +61 303 has shown the radio emission to come from angular scales smaller than about about 7 mas (projected size 14 AU at an assumed distance of 2 kpc). Rea *et al* suggest that X-ray emission of $LSI + 61^o$ 303 must necessarily come from the collision between winds or from the internal wind zone shock region instead of the magnetosphere of the supposed pulsation using Deep Chandra observations of TeV binaries [8]. Dhawan *et al* concluded that the radio and TeV emissions from $LSI + 61^o$ 303 are origi-

 © 2024 Dept. of Physics, NBU

TABLE I: *Mode specific parameters for EPIC PN camera*

| Obs. Mode | Time Resolution | Live Time [%] | MRC diffuse $sec^{-1}$ | MRC point source $sec^{-1}$ |
|---|---|---|---|---|
| Large window | $48ms$ | 94.9 | $1500ms$ | 10 |
| Small window | $6ms$ | 71.0 | $12000ms$ | 100 |
| Timing | $0.03ms$ | 99.5 | $N/A$ | 800 |
| Burst | $7\mu s$ | 3.0 | $N/A$ | 60000 |

MRC= Maximum Count Rate

TABLE II: *Observation data considered for analysis with their* $\phi_{orb}$

| Observation ID | MJD | Exposure | window | $\phi_{orb}$ | Date |
|---|---|---|---|---|---|
| 0112430401(X1) | 52533 | 59999 | PN Small | 0.97 | 09/16/2002 |
| 0207260101(X2) | 53397 | 49972 | PN Small | 0.60 | 01/27/2005 |
| 0505980901(X3) | 54349 | 09860 | PN Large | 0.51 | 09/06/2007 |
| 0505981401(X4) | 54354 | 12293 | PN large | 0.70 | 09/11/2007 |

MJD = Modified Julian Day

The orbital phases $\phi_{orb}$ are computed using $MJD = 43366.275$ and $P_{orb} = 26.496$

nated by the interaction of the wind of a young pulsar with that of the stellar companion [9]. While, Sarkar *et al* based on their studies suggested that particle acceleration sites can be different for events with and without flares, as in Microquasar model, in which the flaming radiation can come from hot spots located above the black hole using RXTE Mission Data. While stationary emissions are due to jets [10]. Kravtsov *et al* in 2020 [11] done studies on the orbital variability and confirm the existence of super-orbital variability using Optical measurements perform with the broad-band BVR polarimeter Dipol-2.

This Be star binary was observed with XMM EPIC PN camera in different modes Table I. Here, in this work, we have considered two modes prime small window as well as prime large window Fig. 1 using medium filter from 2001 to 2007, Some of which are taken as a part of the observational campaign of the system using XMM-Newton [12]. Here, we have considered four observation for our study as mentioned in Table II. Out of four two are in small window mode and two are in large window mode with medium filter. The first observation was made during from 02:23:47.000 hrs of 16th September 2002 to 04:11:28.000 hrs of 16th September 2002 for total $6.426 \times 10^3$ sec with the observation ID 0112430401, the second with observation ID 0202760301 was made during from 17:40:46.000 hrs of 27th Jan 2005 to 07:41:04.000 hrs of 27th Jan 2005 for total $50.418 \times 10^3$ sec, the third with observation ID 0505980901 was made during from 01:31:25.000 hrs to 05:15:02.000 hrs of 6th September 2007, the fourth with observation ID 0505981401 was made during from 01:27:25.000 hrs to 05:29:20.000 hrs of 11th September 2007.

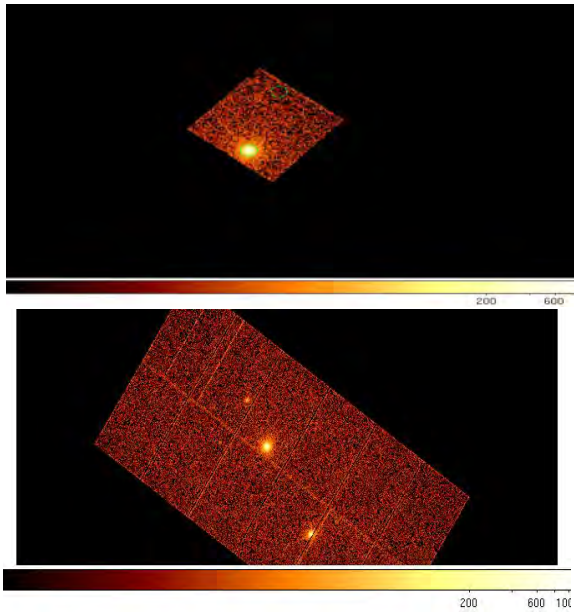

FIG. 1: Spectral Image of LSI $+61^{O}$ 303 in Small Window Mode [Top] and Large window mode [Bottom].

## II. DATA REDUCTION, ANALYSIS & OBSERVATIONS

LS I +61 303 was observed with $XMM-Newton$ EPIC cameras for different time intervals in various windows mode with medium filters in between 2001 to 2007. Here, for study purpose, we have considered few suitable observations. Out of the four data sets, two data sets (0207260101, 0505980901) were having flaring regions at the beginning of the light curve. In this present work, we have processed the data giving special attentions to these regions. For data analysis, we have used XMM Science Analysis System. During data reduction, we have used the SAS's task "epchain" for extraction of EPIC PN camera data. The data was further filtered to include only science events and for patterns less than or equal to $4$ in the energy range from 0.2-15 $keV$. Source spectrum was extracted from a circular region of radius 30 arc-sec around the source position using SAO Image Analysis Software ds9. Background PN spectra was extracted from nearby, source free regions having low value of counts, about $.1\%$ of the central region located at approximately the same readout position as that for the source circle.

### A. Spectral analysis

To obtain the data for spectral analysis, the extracted regions for the source and background spectra as given above is required. Now, one can obtain the related response files using the task 'especget' or using OGIP Spectral Products of 'xmmselect' in Graphical User Interface (GUI). In GUI, the user can

TABLE III: *Best fit results of Spectral analysis with wabs *(po)*

| ID | grouping of energy bin | Powerlaw Index | $\chi^2_{red}$ | $Flux^{**}$ | $Lumin^{*}$ $10^{+33} ergs.sec^{-1}$ |
|---|---|---|---|---|---|
| X1 | gr 0 4095 5 | $1.55^{+}_{-}0.02$ | 406.49/378 | 14.139 | 6.8437 |
| X2 | gr 0 4095 5 | $1.67^{+}_{-}0.01$ | 438.32/378 | 08.622 | 4.1707 |
| X3 | gr 0 4095 5 | $1.72^{+}_{-}0.02$ | 448.92/378 | 08.111 | 3.9234 |
| X4 | gr 0 4095 5 | $1.67^{+}_{-}0.01$ | 400.57/378 | 08.302 | 4.0158 |
| X1 | gr min 35 | $1.48^{+}_{-}0.02$ | 215.82/217 | 15.058 | 7.2838 |
| X2 | gr min 35 | $1.66^{+}_{-}0.02$ | 855.90/812 | 08.588 | 4.1542 |
| X3 | gr min 35 | $1.67^{+}_{-}0.02$ | 265.88/260 | 08.458 | 4.0914 |
| X4 | gr min 35 | $1.64^{+}_{-}0.01$ | 410.22/387 | 08.455 | 4.0901 |

$N_H = 0.5 \times 10^{22}/cm^2$

* Luminosity is calculated for assume distance of 2 kpc.

** Flux measured in unit of $10^{-12} ergs.cm^{-2}.sec^{-1}$

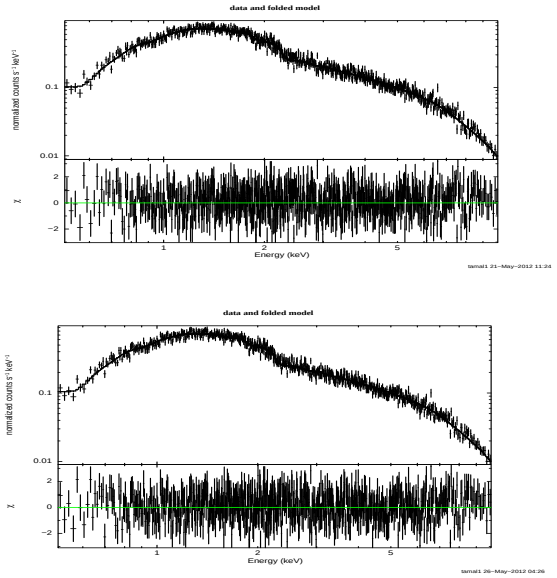


FIG. 2: Spectrum showing the normalized counts per second per keV Vs Energy in keV for model wabs*(powerlaw) for observation ID 0207260101 with Chi square for Flare region [TOP] and Flare free region[BOTTOM].

interactively define the source and background regions.

The GUI mode is provides more flexibility compare to command line in extraction of the spectra. Accordingly we have used the GUI. After using the above task four output files were obtained. They are source spectrum file; background spectrum file, ancillary response file and redistribution matrix file. The next job is to analysis the spectra which can be done using the standard package like xspec for X-ray spectral analysis.

TABLE IV: *Best fit results of Spectral analysis with wabs *(po) allowing $N_H$ to vary*

| ID | $N_H$ | Powerlaw | $\chi^2_{red}$ | $Flux^*$ | $Lumin^{**}$ |
|---|---|---|---|---|---|
| | $10^{22}/cm^2$ | Index | | | $10^{+33}ergs.sec^{-1}$ |
| $X1^{@}$ | 0.598 | $1.67^{+}_{-}0.02$ | 371.68/380 | 13.880 | 6.8437 |
| $X2^{@}$ | 0.512 | $1.69^{+}_{-}0.02$ | 431.62/377 | 08.587 | 4.1707 |
| $X3^{@}$ | 0.500 | $1.72^{+}_{-}0.02$ | 448.92/377 | 08.111 | 3.9234 |
| $X4^{@}$ | 0.516 | $1.69^{+}_{-}0.02$ | 398.22/377 | 08.272 | 4.0158 |
| $X1^{@@}$ | 0.562 | $1.55^{+}_{-}0.02$ | 204.35/217 | 14.872 | 7.2838 |
| $X2^{@@}$ | 0.513 | $1.67^{+}_{-}0.02$ | 853.84/809 | 08.564 | 4.1542 |
| $X3^{@@}$ | 0.492 | $1.65^{+}_{-}0.02$ | 263.82/259 | 08.477 | 4.0914 |
| $X4^{@@}$ | 0.494 | $1.63^{+}_{-}0.01$ | 410.15/384 | 08.456 | 4.0901 |

$^{*}$ Flux measured in unit of $10^{-12}ergs.cm^{-2}.sec^{-1}$

$^{**}$ Luminosity is calculated for assume distance of 2 kpc and $N_H = 0.5 \times 10^{22}/cm^2$.

$^{@}$ Obtained using gr 0 4095 5

$^{@@}$Obtained using gr min 35

Before going for such an analysis, the created spectrum was grouped (binned) depending on the available signal to noise ratio in the data and the science the user wants to perform. The FTOOLS task grppha allows regrouping of the source spectrum based on different criteria. In our case, we have divided the spectrum with flare into two parts i.e one with flare and other with no flare and done the analysis for an energy range of 0.5-10.0 keV Fig. 2. Initially, the spectrum was fitted with a powerlaw(po). Then, other models such as the black body, the gauss(ga) and the multicolor disc black body (diskbb) were tried. It is found that the model multiplicative absorption model "wabs" was used along-with a powerlaw wabs*(po) works well for the source for all data set to fit the spectrum. The best fit parameters along with $\chi^2_{red}$ are given in Table III and Table IV.

### B. Timing analysis

Data for timing analysis were reduced using the XMM Newton Scientific Analysis Software package. The EPIC pn background subtracted light curves in two energy ranges (0.5 to 2.0 keV and 2.0 to 10.0 keV) are reported and the Light curves are plotted for all the data sets along with Hardness ratio and cross correlation as shown in Fig. 3 and Fig. 4, respectively.

The observed X-Ray datas also shows the presence of flaring events which was reported in past also one such report is reported by Smith *et al* [13].

In the Fig. 4, the cross correlation for flaring region and flare free regions are shown and it indicates a

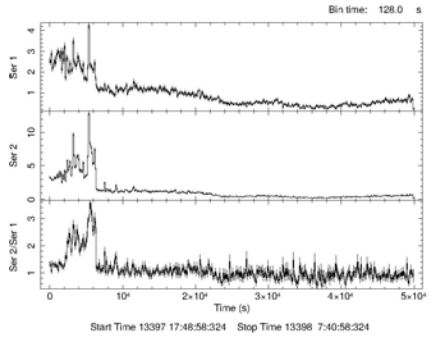


FIG. 3: $LSI + 61^o$ 303 light curve and hardness ratio for observation ID 0207260101.

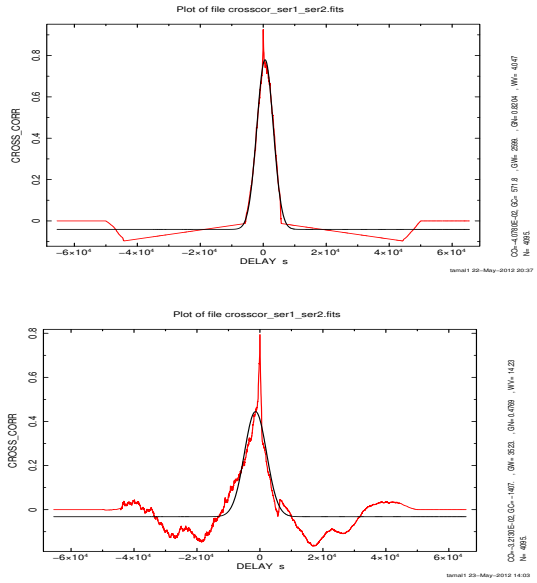


FIG. 4: $LSI+61^o$ 303 cross-correlation for observation ID 0207260101 flare [TOP]and flare free regions[BOTTOM].

clear difference in pattern and same has been discuss in the next section.

## III. DISCUSSION

We found that there is no appreciable change in the average flux for a particular orbital phase band.The spectra for different observation period exhibit power law (without break) feature along with observation. The power index varies with orbital phase; the spectrum is harder at brighter stage. However, the difference in spectral index between low and high emission phase decreases if the absorbing material is considered as variable rather than fixed as done in most of the analysis. We notice a flaring feature at the beginning of two observations . Such a feature was previously noticed in one of the BeppoSAX observation [12]. The flaring and increase of flux in observation ID X1 with $\Phi_{orb} = 0.97$ may be explained using two-accretion

peak model with Inverse Compton [14] , as per which the accretion rate might develop two peaks along the eccentric orbit . It may be noted that $LSI + 61\ 303$ is a X-Ray binary with an eccentric orbit $e = 0.7$. As per two-accretion peak model, the rate of accretion i.e $\frac{dM}{dt} \propto \rho_w / v_{rel}^3$, where $\rho_w$ = density of the straitified wind of the B0 Ve star and $v_{rel}$ = Relative velocity between the wind and the orbiting accretor. The accretion rate may peak depending upon $\rho_w$ and $v_{rel}$ i.e when the density is highest or $v_{rel}$ is lowest.

## IV. SUMMARY

The X-Ray flux (0.5-10 KeV) is found to be highest and spectral Power-law Index ($\Gamma$) is lowest for $\Phi_{orb} = 0.97$ with the two grouping scheme as shown in Table III and Table IV, respectively. It is found that the best fit results of this spectral analysis with wabs*(po) allowing $N_H$ to vary (see Table IV). With grouping scheme "$gr0\ 4095\ 5$", it is observed that there is clear variation of $\Gamma$ , flux and $N_H$ with orbital phase $\phi_{orb}$. The $\Gamma$ has highest value whereas $N_H$ and flux has lowest at $\phi_{orb} = 0.5$ for observation ID X3. However, if we considered the grouping scheme "gr min 35", there is no such variation of $\Gamma$ , but, clear variation of $N_H$ is seen. Under these grouping scheme, the variation or decay in $N_H \approx 0.562\text{-}0.492 = .07 \times 10^{22} cm^{-2}$.Taking the mean density of the disk to be $n_0 \approx 10^9 cm^{-3}$ [6], we get the size of the clumps $s = N_H / n_0 \approx 7 \times 10^{11} cm$ which is comparable with the radius of the Be Star if we assume the the presences of clumps of highly or partially ionised hydrogen. With this simple model, the variation of $N_H$ with $\phi_{orb}$ as observed can be explained on the basis of presence of clumps. In the present work, we have mentioned about the presence of flaring in the Observation ID X1 and X3. Fig. 3 indicates one such event. During such flaring behavior, the hardness ratio is found to increase as in Fig. 3, implying short bursts of high energy radiation as shown in Fig. 4. It indicates that lagging of soft X-Rays during flaring and lagging of hard X-Rays in the flare free event which may be due to the different sites of particle acceleration for flaring and flare free events.

* Electronic address: ta.sa.nbu@hotmail.com

[1] G. Dubus, A&A, **456**, 801 (2006).

[2] M. Chernyakova *et al*, MNRAS, **372**, 1585 (2006).

[3] D. B. Kieda, VERITAS Collaboration, 36th ICRC2019.

[4] P. C. Gregory and A. R. Taylor, Nature, **272**, 704 (1978).

[5] P. C. Gregory, ApJ, **575**, 427 (2002).

[6] M. Chernyakova *et al*, MNRAS, **470**, 1718 (2017).

[7] Albert, J. *et al*, ApJ, **674**, 1037 (2008).

[8] N. Rea, *et al*, MNRAS, **405**, 2206 (2010).

[9] V. Dhawan, A. Mioduszewski, and M. Rupen, VI Microquasar Workshop: Microquasars and Beyond, 52.1 (2006).

[10] T. Sarkar, *et al*, RAA, **16**, 104 (2016).

[11] V. Kravstov *et al*, A&A, **643**, A170 (2020).

[12] Sidoli, L.Pelliizoni, *et al*, A&A **459**, 901 (2006).

[13] A. Smith *et al*, ApJ, **693**, 1621 (2009).

[14] M. Massi *et al*, MNRAS, **498**, 3592 (2020).